Nonlinear magnetic responses at the phase boundaries around helimagnetic and skyrmion lattice phases in MnSi: Evaluation of robustness of noncollinear spin texture

K. Tsuruta,[1] M. Mito,[2,3,*] H. Deguchi,[2] J. Kishine,[3,4] Y. Kousaka,[3,5] J. Akimitsu,[5] and K. Inoue[3,6,7]

[1]*Japan Synchrotron Radiation Research Institute (JASRI), Hyogo 679-5198, Japan*
[2]*Graduate School of Engineering, Kyushu Institute of Technology, Kitakyushu 804-8550, Japan*
[3]*Chirality Research Center, Hiroshima University, Higashihiroshima 739-8526, Japan*
[4]*Graduate School of Arts and Sciences, The Open University of Japan, Chiba 261-8586, Japan*
[5]*Research Institute for Interdisciplinary Science, Okayama University, Okayama 700-8530, Japan*
[6]*Graduate School of Science, Hiroshima University, Higashihiroshima 739-8526, Japan*
[7]*Institute for Advanced Materials Research, Hiroshima University, Higashihiroshima 739-8526, Japan*

(Received 25 August 2017; published 13 March 2018)

The phase diagram of a cubic chiral magnet MnSi with multiple Dzyaloshinskii-Moriya (DM) vectors as a function of temperature T and dc magnetic field H_{dc} was investigated using intensity mapping of the odd-harmonic responses of ac magnetization ($M_{1\omega}$ and $M_{3\omega}$), and the responses at phase boundaries were evaluated according to a prescription [J. Phys. Soc. Jpn. **84**, 104707 (2015)]. By evaluating $M_{3\omega}/M_{1\omega}$ appearing at phase boundaries, the robustness of noncollinear spin texture in both the helimagnetic (HM) and the skyrmion lattice (SkL) phases of MnSi was discussed. The robustness of vortices-type solitonic texture SkL in MnSi is smaller than those of both the single DM HM and chiral soliton lattice phases of a monoaxial chiral magnet $Cr_{1/3}NbS_2$, and furthermore the robustness of the multiple DM HM phase in MnSi is smaller than that of its SkL. Through magnetic diagnostics over the wide T-H_{dc} range, we found a new paramagnetic (PM) region with ac magnetic hysteresis, where spin fluctuations have been observed via electrical magnetochiral effect. The anomalies observed in the previous ultrasonic attenuation measurement correspond to the peak positions of out-of-phase $M_{1\omega}$. The appearance of a new PM region occurs at a characteristic magnetic field, above which indeed the SkL phase appears. It has us suppose that the new PM region could be a phase with spin fluctuation like the skyrmion gas phase.

DOI: 10.1103/PhysRevB.97.094411

I. INTRODUCTION

Solitonic features in spin systems, such as isolated domains, kinks, and vortices, have been attractive in the field of spintronics, and the spin solitonic texture accompanies noncollinear magnetic texture [1]. In particular, a spin solitonic object created by the Dzyaloshinskii-Moriya (DM) interaction originating in the spin-orbit interaction [2,3] is a hot topic. Quantitative evaluation of the nonlinear phenomena due to noncollinear spin texture seen there [1] is an important subject of basic science to utilize the solitonic features in spintronics devices and understand the concept of nonlinearity in diverse scientific topics, including liquid crystals. Below, two types of spin solitonic texture are reviewed.

A one-dimensional (1D) solitonic texture is constructed in monoaxial chiral magnets such as $Cr_{1/3}NbS_2$ [4]. At zero dc magnetic field (H_{dc}), a three-dimensional spin-modulated structure, called a helimagnetic (HM) structure [Fig. 1(a)], is stabilized. The magnetization curve for H_{dc} of arbitrary strength and direction has been known to be reproduced with a Heisenberg spin model with DM interactions and magnetocrystalline anisotropy [5]. In particular, when H_{dc} is applied perpendicular to the chiral helical axis, a superlattice consisting of a 2π-twisting and ferromagnetic (FM) array, termed the chiral soliton lattice (CSL) [Fig. 1(b)], is realized. When this superlattice is viewed from the side of the forced ferromagnet (FFM) [like Fig. 1(c)], this 2π twisting can be considered as a type of topological magnetic soliton (TMS). In this situation, we can change the spin solitonic feature as a function of H_{dc}, such that the number of TMSs is manipulated by the magnitude of H_{dc} [6].

By contrast, the two-dimensional (2D) solitonic texture is the skyrmion lattice (SkL) consisting of cylindrical spin vortices [Fig. 1(d)], which is stabilized in cubic chiral magnets [7,8]. Theoretical studies in this area began approximately 30 years ago [9–12]. There have been many experimental studies of MnSi [13,14], $Fe_{0.5}Co_{0.5}Si$ [15], FeGe [16], Cu_2OSeO_3 [17], and PdFe/Ir(111) [18,19] to date. Historically, the first observation concerning this subject was the discovery of the so-called "A phase" of the bulky MnSi crystal in 1977 [20]. It exists in narrow temperature (T) and H_{dc} regions. Indeed, the SkL phase was observed as a down pocket of magnetization and magnetic susceptibility in T and H_{dc} scans (for instance, MnSi [21], FeGe [22]). Figure 2 shows the T-H_{dc} phase diagram of prototype materials such as MnSi and FeGe recognized widely thus far [21,23]. The T-H_{dc} regions of HM, conical magnetic (CM), intermediate (IM), paramagnetic (PM), and SkL phases were determined by several experimental approaches such as magnetic susceptibility [21,22], ultrasonic attenuation [24,25], heat capacity [26,27], and magnetoresistance [28]. The boundary between the FFM (elsewhere termed field-polarized region)

*mitoh@mns.kyutech.ac.jp

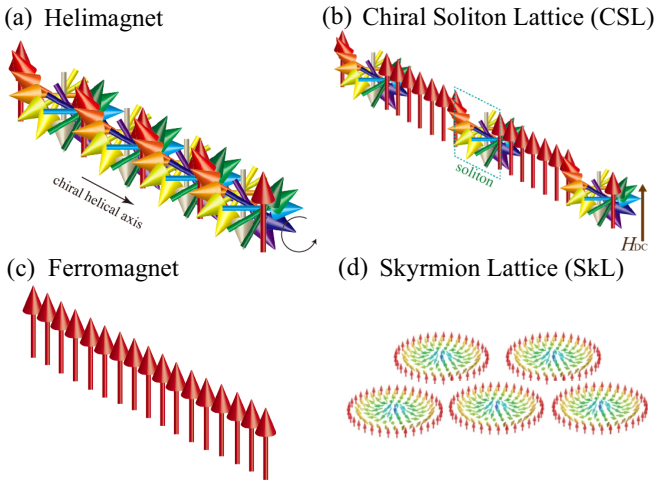

FIG. 1. Spatial location of spin phase orders: (a) noncollinear helimagnet, (b) noncollinear chiral soliton lattice (CSL), (c) collinear ferromagnet, and (d) noncollinear skyrmion lattice (SkL).

and PM regions has not been determined in MnSi via magnetic measurements. The origin of the green line in the PM region, obtained by in-phase ac susceptibility (in FeGe) [22], the ultrasonic attenuation measurements (in MnSi) [24,25], and heat capacity (in FeGe) [26,27] has not been verified in previous studies. The precursor phenomena seen there have also been pointed out via the small angle neutron scattering of MnSi [29]. Recently, in MnSi, the second harmonic resistivity reflecting spin fluctuation was observed in a certain region near the broken green line [28]. Indeed, in the film, a skyrmion gas (melting state of SkL) has been predicted in the corresponding region [30]. Thus, the phase diagram concerning HM, CM, IM, and SkL phases is reliable, whereas there is room for discussion regarding the stability of SkL including the existence of a unique anomaly line in the PM phase.

Thus, in both 1D and 2D textures, the TMS becomes an important object in stabilizing a noncollinear magnetic structure. Experimentally, neutrons become a promising probe for detecting the TMSs [29,31,32], while it is also meaningful to investigate the robustness of the spin phase order against external magnetic fields using conventional tools.

Indeed, in the aforementioned $Cr_{1/3}NbS_2$, prominent third-harmonic magnetic responses have already been detected at the phase (region) boundaries between HM [Fig. 1(a)] and PM states and between the CSL [Fig. 1(b)] and FFM [like Fig. 1(c)] states [33]. This third-harmonic response is not restricted to the spin system, but it has already been observed in tilted smectic liquid crystals, i.e., chiral smectic phase [34–40]. A large third-harmonic dielectric response due to the softening of tilt fluctuation called "soft mode" is also observed in the smectic liquids with a short-pitched incommensurate helical structure over several layers [40]. The nonlinear dynamics reflects the material constants such as spontaneous polarization and viscosity [40]. Thus, previous studies imply that the third-harmonic response is related to the formation of domains with incommensurate helical structure, and it reflects the thermal fluctuation of the domain formation, namely the softening. This relationship is surely a common feature in both magnetic and liquid crystals.

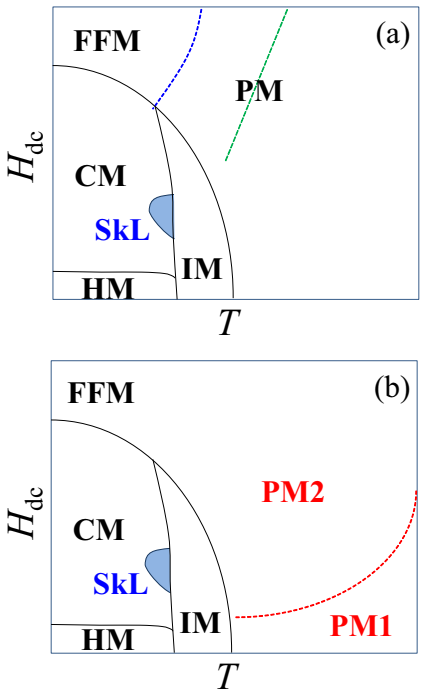

FIG. 2. (a) T-H_{dc} phase diagram of B20-type chiral magnets such as MnSi and FeGe recognized thus far via a series of studies for bulk crystals [21,23,26]. The description of each phase is HM: helimagnetic phase, CM: conical magnetic phase, SkL: skyrmion lattice phase, IM: Intermediate phase, PM: paramagnetic phase, and FFM: forced ferromagnetic region (elsewhere often termed field-polarized region). The anomalies in the in-phase ac magnetic susceptibility (FeGe [22]), ultrasonic attenuation (MnSi [24,25]), and heat capacity (FeGe [26,27]) measurements were observed near the broken green line. The second harmonic resistivity in MnSi was observed in a certain region near the broken green line [28]. In MnSi, the boundary between FFM and PM has not been determined experimentally. (b) T-H_{dc} phase diagram of MnSi determined via the present study. Here the PM region in (a) is divided into two regions (i.e., PM1 and PM2).

Given this background, it is fruitful to study the spin phase coherence related to the 2D TMSs in terms of higher-order harmonic magnetic responses. In this study, the third-harmonic magnetic response in MnSi is compared with those of other helical spin systems in order to semiquantitatively discuss the robustness of the spin phase order in the SkL. Furthermore, through the systematical magnetic diagnostics based on a prescription [41], the T-H_{dc} diagram will be verified in detail, and a new magnetic region will be pointed out experimentally.

II. NONLINEAR AC MAGNETIC RESPONSES

Below, let us review a method to evaluate the magnetic nonlinearity semiquantitatively [41]. The ac magnetic response M_{ac} under an ac magnetic field $H_{ac} = h\sin(\omega t)$, where h is the amplitude of H_{ac}, ω $(= 2\pi f)$ is the angular frequency (f is the frequency), and t is the time, is expanded as

$$M_{ac}(t) = M_{1\omega}\sin(\omega t + \theta_{1\omega}) + M_{2\omega}\sin(2\omega t + \theta_{2\omega}) + M_{3\omega}\sin(3\omega t + \theta_{3\omega}) + \cdots, \quad (1)$$

TABLE I. Typical ac magnetic responses obtained according to the prescription proposed in Ref. [41]. $M_{1\omega}$ and $M_{3\omega}$ are the amplitudes of the first and third harmonic components, respectively. H_c is a coercive field in the M_{ac} vs H_{ac} profile, and h is the amplitude of H_{ac}. $M'_{1\omega}$ and $M''_{1\omega}$ are the in-phase and out-of-phase components of the first harmonic component, respectively. Both γ and η appear in the Duffing equation of Eq. (2).

Type	$M_{3\omega}/M_{1\omega}$	H_c/h	$M''_{1\omega}/M'_{1\omega}$	γ	η
1	0	0	0	0	0
2	0	$\neq 0$	$\neq 0$	$\neq 0$	0
3	<0.05	>0.5	$\neq 0$	$\neq 0$	$\neq 0$
4	$\geqslant 0.05$	>0.1	$\neq 0$	$\neq 0$	$\neq 0$
5	$\geqslant 0.05$	$\leqslant 0.1$	~ 0	$\neq 0$	$\neq 0$

where $M_{n\omega}$ (where n is an integer) represents the nth harmonic component, and $\theta_{n\omega}$ (<0) is the phase delay of each $M_{n\omega}$ against H_{ac}. Representative in-phase and out-of-phase components are as follows: $M'_{1\omega} = M_{1\omega}\cos\theta_{1\omega}$, $M''_{1\omega} = -M_{1\omega}\sin\theta_{1\omega}$, and $M'_{3\omega} = M_{3\omega}\cos\theta_{3\omega}$. The anomaly in $M_{3\omega}$ appears at any phase boundary, and reflects the thermal fluctuation of magnetic domains near the phase transition: For instance, $M_{3\omega}$ due to the formation of long-range magnetic order accompanies a large phase change against T scanning across the magnetic ordering temperature (T_c), whereas the glassy $M_{3\omega}$ due to magnetic frustration between magnetic domains does have a small phase change [42–47]. Thus, the robustness of the spin phase order can be studied via $M_{3\omega}$.

By associating these ac magnetic responses with a mechanical spring model, $M_{3\omega}$ is connected with the nonlinear ηx^3 term of the following mechanical nonlinear spring equation (the so-called Duffing equation) [41]:

$$\frac{d^2x}{dt^2} + 2\gamma\frac{dx}{dt} + \omega_0^2 x + \eta x^3 = F\sin\omega t, \qquad (2)$$

where x is the position of a material (here, a domain wall) with a mass m connected to a spring (spring constant k) [48]. In Eq. (2), $\omega_0 = (k/m)^{1/2}$. The quantity $M_{3\omega}/M_{1\omega}$ is called the Klirr factor, and it represents the ratio of the strain in the periodic $M_{ac}(t)$ response [41,48]. In a reference study on MnP, we classified the typical responses into five groups, as shown in Table I [41]; types 1 and 2 appear for $\eta = 0$, and type 1 further requires $\gamma = 0$. As η increases, the types are transformed as $3 \rightarrow 4 \rightarrow 5$. Note that the ultimate group, type 5, with huge η, has no ac hysteresis (i.e., the coercive field $H_c \approx 0$ in the M_{ac} vs H_{ac} profile and no $M''_{1\omega}$). Thus, magnetic diagnostics using mainly $M_{3\omega}$ and $M''_{1\omega}$ can be valid for a magnetic study of unique magnetic domains [41,49–54]. In particular, $M_{3\omega}/M_{1\omega}$ is closely related to η.

Our present interest is whether we can observe magnetic nonlinearity due to the SkL formation. First, we confirm the phase boundary on the T-H_{dc} phase diagram in a bulk single crystal of MnSi using $M'_{1\omega}$, $M''_{1\omega}$, and $M_{3\omega}$, so that a new magnetic region will be pointed out in the PM region. Next, we diagnose the magnetic dynamics near both HM and SkL phases, and discuss the robustness of the noncollinear spin texture consisting of topological objects.

III. EXPERIMENTAL PROCEDURE

A single crystal of MnSi was synthesized by a procedure described elsewhere [55], and the size was approximately $2.4 \times 0.6 \times 0.6$ mm^3. The ac magnetic response (M_{ac}) was observed using a superconducting quantum interference device (SQUID) magnetometer (Quantum Design Inc.) equipped with an ac measurement option. The main f of H_{ac} was 10 Hz, and h was 3.9 Oe. The phase diagram of a bulky single crystal is known to be almost independent of the direction of H_{dc} applied for the crystal axes [21] (indeed, the region of SkL slightly depends on the direction of H_{dc}). Herein, both H_{ac} and H_{dc} were applied parallel to the [111] direction. There are two kinds of measurement sequences: (1) the increment of H_{dc} at a fixed T after zero-field cooling from the above T_c (Sec. IV A) and (2) the increment of T at a fixed H_{dc} after zero-field cooling from the above T_c (Sec. IV B). The SQUID voltage proportional to $M_{ac}(t)$ can be obtained by using the SQUID magnetometer software. The number of the data points in one period of $M_{ac}(t)$ depends on f. Each $M_{n\omega}$ was evaluated by spectral analysis of the time-dependent SQUID voltage using software originally developed for Fourier transformations. In the final step, the existence of each $M_{n\omega}$ was confirmed by comparing the combination of wave forms of prominent $M_{n\omega}$'s with the observed wave form of SQUID voltage. The series of ac responses obtained above were diagnosed according to the prescription described in the literature of Ref. [41].

IV. EXPERIMENTAL RESULTS

A. Scanning as a function of dc magnetic field

To locate two phase boundaries between the HM and CM phases and between the CM and SkL phases, the results of scanning H_{dc} after zero-field cooling are presented. Figures 3(a)–3(c) show the H_{dc} dependence of $M'_{1\omega}$ (a), $M''_{1\omega}$ (b), and $M_{3\omega}$ (c) at temperatures ranging from 27.5 to 28.7 K. As seen in Fig. 3(a), as H_{dc} increases from zero, $M'_{1\omega}$ increases from a finite value (0.85 emu/mol), and, at around 200 Oe, it tends to saturate in the level of above 1.11 emu/mol. This behavior corresponds to the spin-flop transition from the HM to the CM phase. For 28.4–28.7 K, $M'_{1\omega}$ exhibits a dip at around $H_{dc} = 1.9$ kOe. This dip indicates the T-H_{dc} region of the SkL surrounded with the CM phase. At approximately 3.5 kOe, $M'_{1\omega}$ decreases with increasing H_{dc}, presenting the feature of the ferromagnetic-domain formation (the FFM region). This decrease in $M'_{1\omega}$ becomes sharp with decreasing T. This transformation from CM to FFM phases has also been detected by the ultrasonic attenuation [24,25].

As seen in Fig. 3(b), $M''_{1\omega}$ shows two sharp anomalies at the boundaries between the CM and SkL phases as well as one distinct cusp at the boundary between the HM and CM phases. The FFM region for $H_{dc} > 3.8$ kOe exhibits a finite plateau accompanying some energy loss [56]. It is noted that the aforementioned results themselves have already been reported [21].

Figure 3(c) shows that the magnitude of $M_{3\omega}$ exhibits a minute anomaly at the boundary between the HM and CM phases. The HM phase of MnSi in zero-field cooling has multiple domains, as the crystal structure of MnSi has multiple screw axes [57]. The small $M_{3\omega}/M_{1\omega}$ ratio of 0.2% level is due

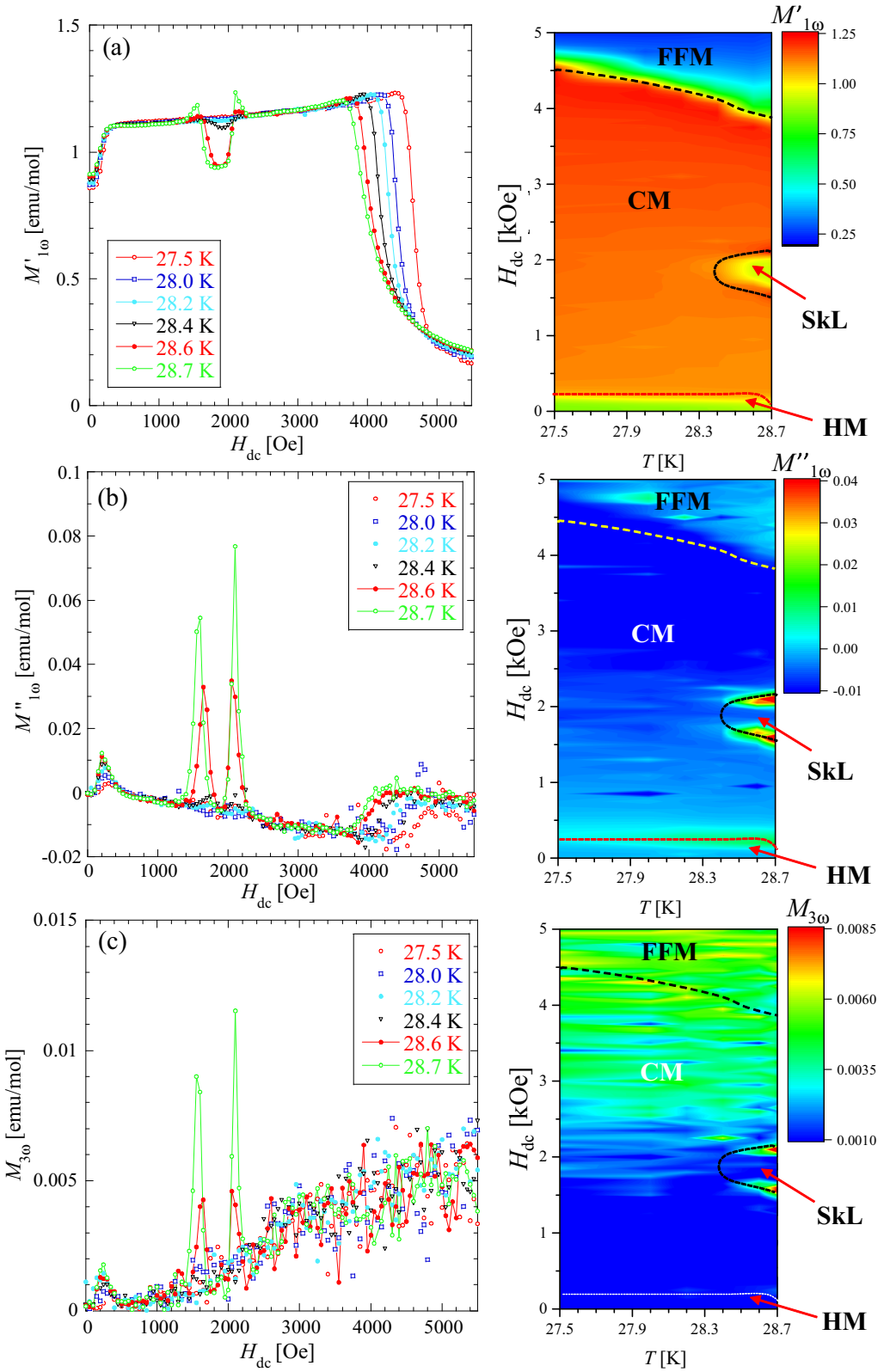

FIG. 3. H_{dc} dependence of ac magnetic responses (a) $M'_{1\omega}$, (b) $M''_{1\omega}$, and (c) $M_{3\omega}$ for one single crystal of MnSi under an ac field with $h = 3.9$ Oe and $f = 10$ Hz. Each figure shows the corresponding intensity map, where the intensity increases as the color changes from blue to red. The description of each phase has been described in the figure caption of Fig. 2.

to a nonsingle HM domain structure by multiple DM vectors. On the other hand, the CM phase has a single domain structure created by field-induced reorientation of the spin helix [57]. There is a distinct change in the spin orientation between the HM and CM phases. Furthermore, $M_{3\omega}$ also exhibits distinct anomalies at the level of $M_{3\omega}/M_{1\omega} \sim 1\%$ at the boundary between the CM and SkL phases. We note that the later CM-SkL boundaries exhibit much larger $M_{3\omega}$ anomaly than that at the former HM-CM boundary.

B. Scanning as a function of temperature

Here we present the phase diagram over a wide T range including the PM region, which was obtained by increasing T at a fixed H_{dc} after zero-field cooling. Figure 4 shows the T dependence of $M'_{1\omega}$ [(a) and (b)], $M''_{1\omega}$ [(c) and (d)], and $M_{3\omega}$ [(e) and (f)] of MnSi for various H_{dc} values. Figures 4(a), 4(c), and 4(e) show the results for $26 \leqslant T \leqslant 35$ K, and Figs. 4(b), 4(d), and 4(f) show those enlarged for $28 \leqslant T \leqslant 30$ K.

First, the T dependence at zero H_{dc} is explained; in the HM region for $T \leqslant 28$ K, $M'_{1\omega}$ is almost constant, and it exhibits a prominent increase at around 29 K. It then exhibits a gradual decrease with increasing T. At $H_{dc} = 0.5$ kOe, the upward change for $28 < T < 29$ K vanishes [see Fig. 4(b)], suggesting the transformation of the ground state from the HM to the CM phase. As H_{dc} increases, the overall changes in $M'_{1\omega}(T)$ shift it toward the low-temperature side. In the process, two new changes appear: (1) A broad hump gradually appears at around 33 K [see Fig. 4(a)], and (2) a temporary drop appears for $T = 28.4$–29.2 K [see Fig. 4(b)]. When f of H_{ac} increases as $1 \rightarrow 10 \rightarrow 100$ Hz, the former slightly shifts toward the high temperature side decreasing the magnitude, as shown in Fig. 5(a) for $H_{dc} = 4.5$ kOe. The latter corresponds to the SkL phase surrounded with both the CM and IM phases. It is noted that the aforemention results themselves have already been reported elsewhere [21].

When these phenomena are observed via the window of $M''_{1\omega}$, $M''_{1\omega}$ presents a broad hump at around 31 K [see Fig. 4(c)] and a quite sharp anomaly at the phase boundary between the CM and SkL phases [see Fig. 4(d)]. They correspond to the aforementioned two changes in $M'_{1\omega}$, (1) and (2), respectively. In particular, the former suggests the existence of a new PM region (termed PM2 later), whose magnetic dynamics is similar to that of an FFM region. Indeed, it is difficult to determine the distinct boundary between FFM and PM2 according to the ac magnetic responses. As seen in Fig. 5(b), the characteristic frequency of magnetic dynamics in PM2 is approximately 10 Hz, which is in the same level of typical domain dynamics [49,52]. The type-2 of magnetic dynamics in PM2 surely originates from any magnetic domain formation: For instance, a cylindrical spin vortex (i.e., skyrmion) can be considered to a kind of domain.

As seen in Figs. 4(e) and 4(f), further observation via the window of $M_{3\omega}$ reveals only a sharp anomaly with a Klirr factor of approximately 1% at the phase boundary between the CM and SkL phases. As seen in Fig. 6, this behavior does not depend on the frequency f (= 1, 10, and 100 Hz) of H_{ac}, suggesting that the SkL phase has a robust spin order against ac fields with amplitudes of as much as 4 Oe. However its $M_{3\omega}$ intensity is smaller than $M_{3\omega}$ observed in $Cr_{1/3}NbS_2$ with the monoaxial DM vector [33]. On the other hand, we find no $M_{3\omega}$ response near the boundary between the HM and IM phases in the T scan. This is because the HM phase is of the multidomain helix type.

Figures 7(a)–7(c) show two-dimensional intensity maps of $M'_{1\omega}$ (a), $M''_{1\omega}$ (b), and $M_{3\omega}$ (c) at $f = 10$ Hz, which are made using the information of Fig. 4. For reference, the anomaly positions of ultrasonic attenuation observed by Kusaka *et al.* [24] are also plotted in all figures. Figures 8(a)–8(c) are the three-dimensional version of Figs. 7(a)–7(c). Herein we reconsider the phase diagram of MnSi as a function of T and H_{dc}. For the CM phase, $M'_{1\omega}$ has an almost constant high intensity, and its intensity is larger in both the HM and SkL phases. The change from CM to FFM accompanies the sharp decrease in $M'_{1\omega}$, and this phase boundary in Figs. 7(a) and 8(a) has also been detected by the ultrasonic attenuation as mentioned above [24,25]. However, the boundary between the CM and SkL phases, as shown in both $M''_{1\omega}$ and $M_{3\omega}$, has sharp anomalies, suggesting the existence of a prominent border between two regions. In $M'_{1\omega}$, the SkL appears just in a single pocket. $M_{3\omega}$ responds only to the change in magnetic domain between the CM and SkL phases as seen in Figs. 7(c) and 8(c). There is no $M_{3\omega}$ anomaly between the SkL and IM phases. Thus, $M_{3\omega}$ appears only at the low temperature side of SkL, and responds to the distinct change in the dimension of spirality from quasi-1D conical spirality to 2D vortex lattice. It is interesting that a hole without intensity appears in both the $M''_{1\omega}$ and $M_{3\omega}$ responses around the vertex of the parabolic boundary [21,58,59]. Furthermore, the boundary on the low-temperature side of the IM phase is sharp, suggesting the existence of a first-order transition. The IM region may act as a buffer region for the first-order transition from the PM to the CM and HM phases. In addition, in Figs. 7(b) and 8(b) we find a characteristic region with finite $M''_{1\omega}$ in the PM region, so that we distinguish the region named PM2 from the PM1 region with no $M''_{1\omega}$.

In the measurements of ultrasonic attenuation of MnSi, the boundaries for CM-FFM, CM-SkL, CM-IM, and IM-PM were observed [24,25]. Except for the boundaries mentioned above, an anomaly line was drawn in the PM region, whereas the origin has not been verified in the previous studies. When compared with the present results of Figs. 7(b) and 8(b), the uncleared line of ultrasonic attenuation is consistent with the broad anomaly of $M''_{1\omega}$. Our data for $H_{dc} > 3.5$ kOe are consistent with the results of Bauer *et al.* [27]. In the present study we determined an almost region of a new PM region using the intensity mapping. Similar anomalies have also been observed in the PM region of FeGe as an anomaly of in-phase magnetic susceptibility [22] and a shoulder of specific heat [26], suggesting that some magnetic entropy remains. Furthermore, the second harmonic resistivity in MnSi also exhibits significant anomaly reflecting spin fluctuation near there [28]. Thus, the intensity mapping of both $M'_{1\omega}$ and $M''_{1\omega}$ perfectly elucidate the boundary between IM and PM. In particular, $M''_{1\omega}$ presents a broad anomaly in PM over a wide H_{dc} region. However, at low H_{dc}'s where SkL appears, the ultrasonic attenuation cannot distinguish between the two above. Now, the intensity mapping of $M''_{1\omega}$ enables us to determine a complex PM region termed PM2. Herein, it is stressed that we paid much attention not to the peak of $M''_{1\omega}$ but the intensity mapping of $M''_{1\omega}$ in order to determine

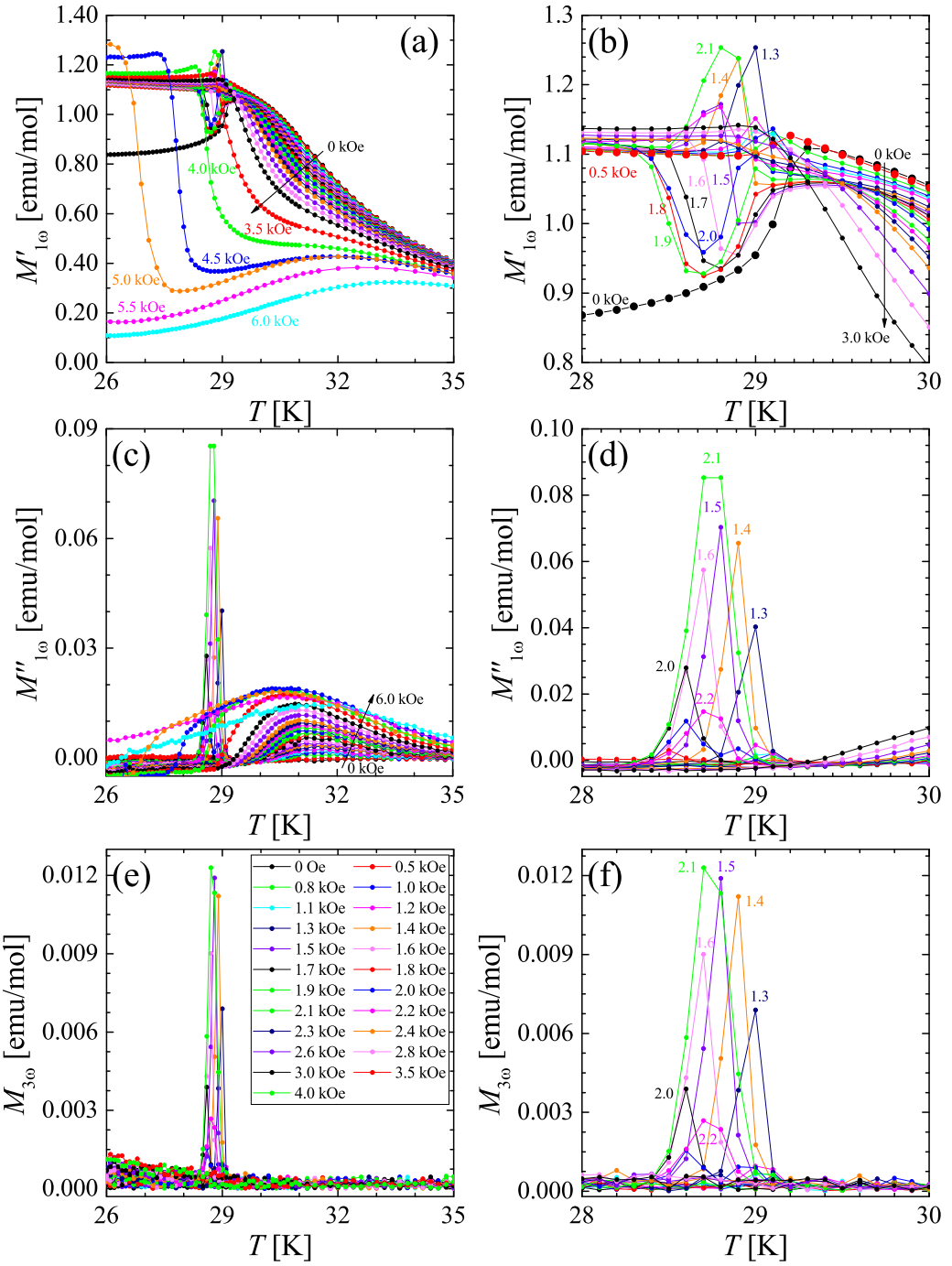

FIG. 4. Temperature dependence of ac magnetic responses (a) and (b) $M'_{1\omega}$, (c) and (d) $M''_{1\omega}$, and (e) and (f) $M_{3\omega}$ for MnSi at various $H_{\rm dc}$ values under an ac field with $h = 3.9$ Oe and $f = 10$ Hz. Both $H_{\rm dc}$ and $H_{\rm ac}$ are applied along the [111] direction.

a characteristic PM region (PM2). Furthermore, the existence of PM2 has forced us to reconsider how the SkL is stabilized at intermediate $H_{\rm dc}$'s near the magnetic ordering temperature.

V. DISCUSSION

The 1D solitonic system $Cr_{1/3}NbS_2$ with the monoaxial DM vector has three well-regulated spin-phase orders such as HM [Fig. 1(a)], CSL [Fig. 1(b)], and FFM [like Fig. 1(c)]. At $H_{\rm dc} = 0$, the transition from the HM to the PM state accompanies a huge $M_{3\omega}$ with a Klirr factor of more than 10%, and its ac response is classified to type 5 [33]. However, a small $H_{\rm dc}$ of a few tens of oersteds makes its $M_{3\omega}$ vanish. Above a critical $H_{\rm dc}$, $M_{3\omega}$ reappears at the phase boundary between the CSL and FFM states, and its ac response is classified to type 4.

Below, we compare the dynamical magnetic response in MnSi with the above-mentioned results for $Cr_{1/3}NbS_2$. In the T scan, an $M_{3\omega}$ response in MnSi was observed not at the boundary between the SkL and IM phases but at the boundary between the CM and SkL phases. In the $H_{\rm dc}$ scan, an $M_{3\omega}$ response also appeared at the border between the HM and CM phases. Figure 9 shows the change in dynamical magnetic

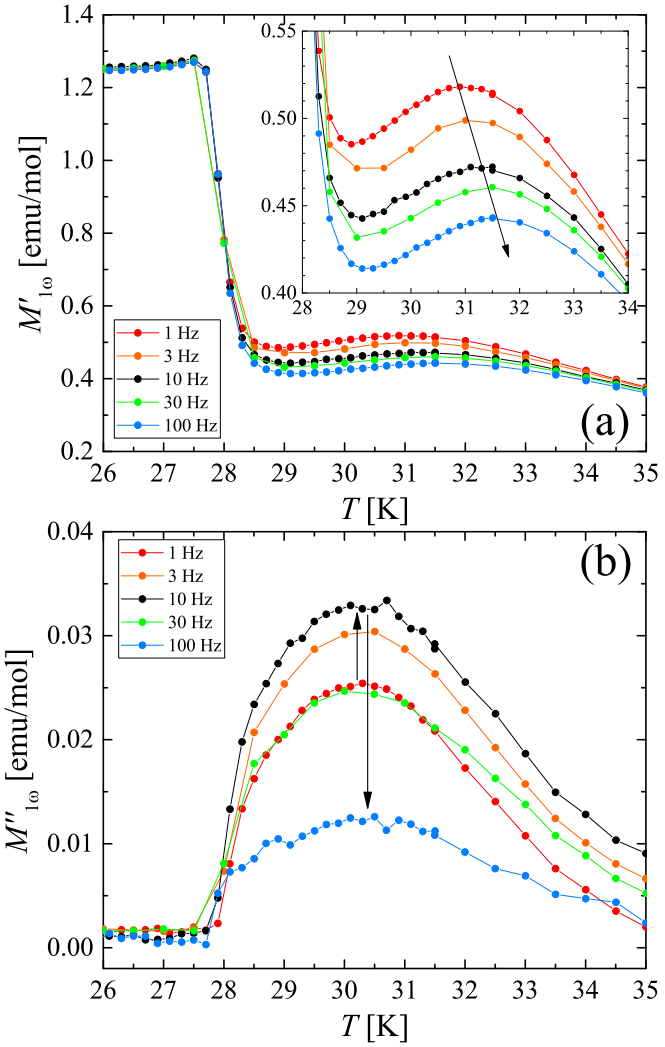

FIG. 5. Temperature dependence of ac magnetic responses (a) $M'_{1\omega}$ and (b) $M''_{1\omega}$ for MnSi at $H_{dc} = 4.5$ kOe under an ac field with $h = 3.9$ Oe and $f =$ 1-100 Hz. Both H_{dc} and H_{ac} are applied along the [111] direction.

response type at six representative H_{dc} values as a function of T. First, as shown Fig. 9(a), HM, IM, and PM1 were stabilized at $H_{dc} < 0.3$ kOe, and they all exhibit the type-1 magnetic dynamics. Next, as shown in Fig. 9(b), CM (type 1) appears instead of HM (type 1) at $0.3 < H_{dc} < 0.8$ kOe. Third, as shown in Fig. 9(c), for $0.8 < H_{dc} < 1.2$ kOe, PM2 (type 2) appears between IM (type 1) and PM1 (type 1). Furthermore, as shown in Fig. 9(d), for $1.2 < H_{dc} < 2.1$ kOe, SkL (type 1) appears between CM (type 1) and IM (type 1), and just at the boundary between CM and SkL, the type-3 response appears sharply. Here the territory of PM2 expands. Note that the SkL itself exhibits a simple linear response against H_{ac}, suggesting a magnetically small viscosity phase. And, as shown in Fig. 9(e), for $2.1 < H_{dc} < 4.0$ kOe, SkL came cleanly out of CM of Fig. 9(d). Finally, as shown in Fig. 9(f), for $H_{dc} > 4.0$ kOe, IM vanishes, and FFM (type 2) appears instead of CM. As mentioned above, it is difficult to draw the boundary between FFM and PM2. Indeed, this boundary seems to be observed in FeGe by the specific heat measurement [26]. The

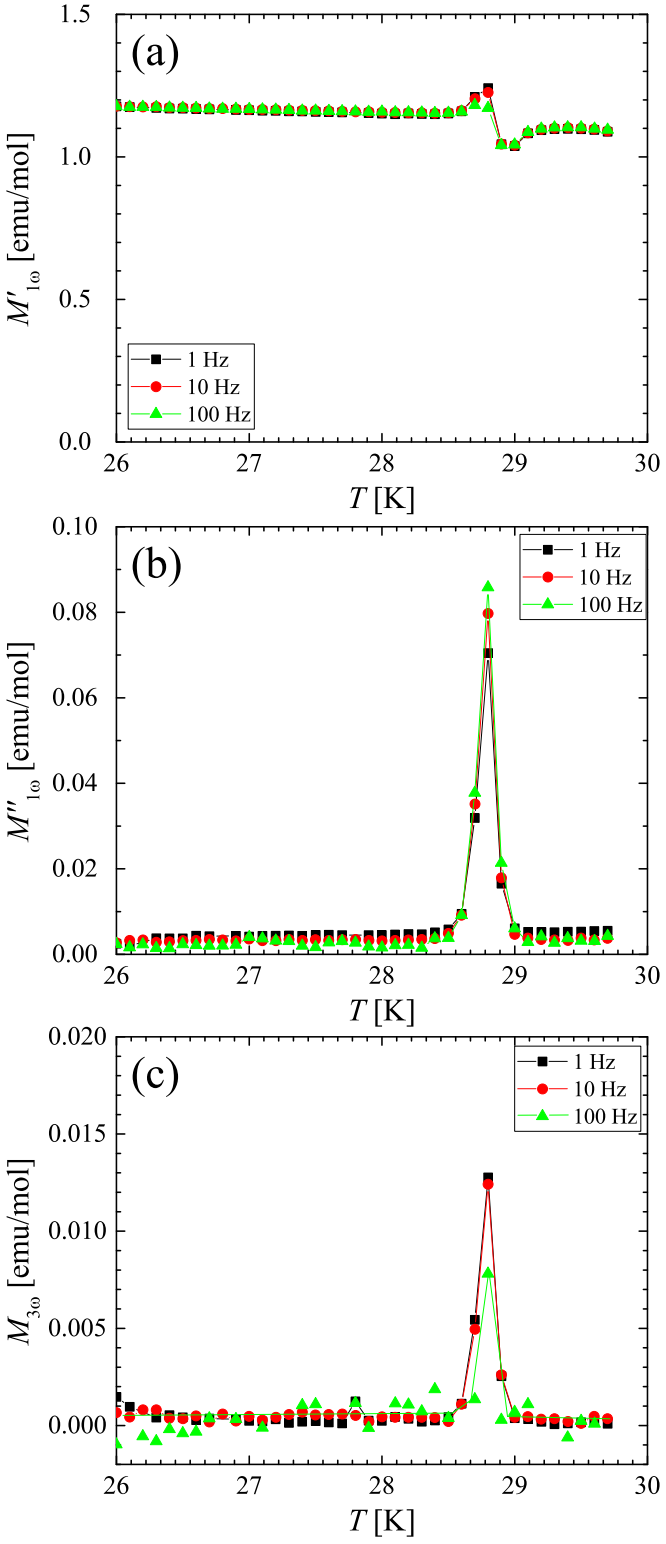

FIG. 6. Temperature dependence of ac magnetic responses (a) $M'_{1\omega}$, (b) $M''_{1\omega}$, and (c) $M_{3\omega}$ for MnSi at $H_{dc} = 1.5$ kOe under an ac field with $h = 3.9$ Oe and $f = 1$, 10, and 100 Hz. Both H_{dc} and H_{ac} are applied along the [111] direction.

position with maximum $M''_{1\omega}$ in the PM2 region of MnSi has already been identified by the ultrasonic attenuation [24,25]. Recently, in MnSi, the second harmonic resistivity reflecting spin fluctuation was observed in a certain region near the

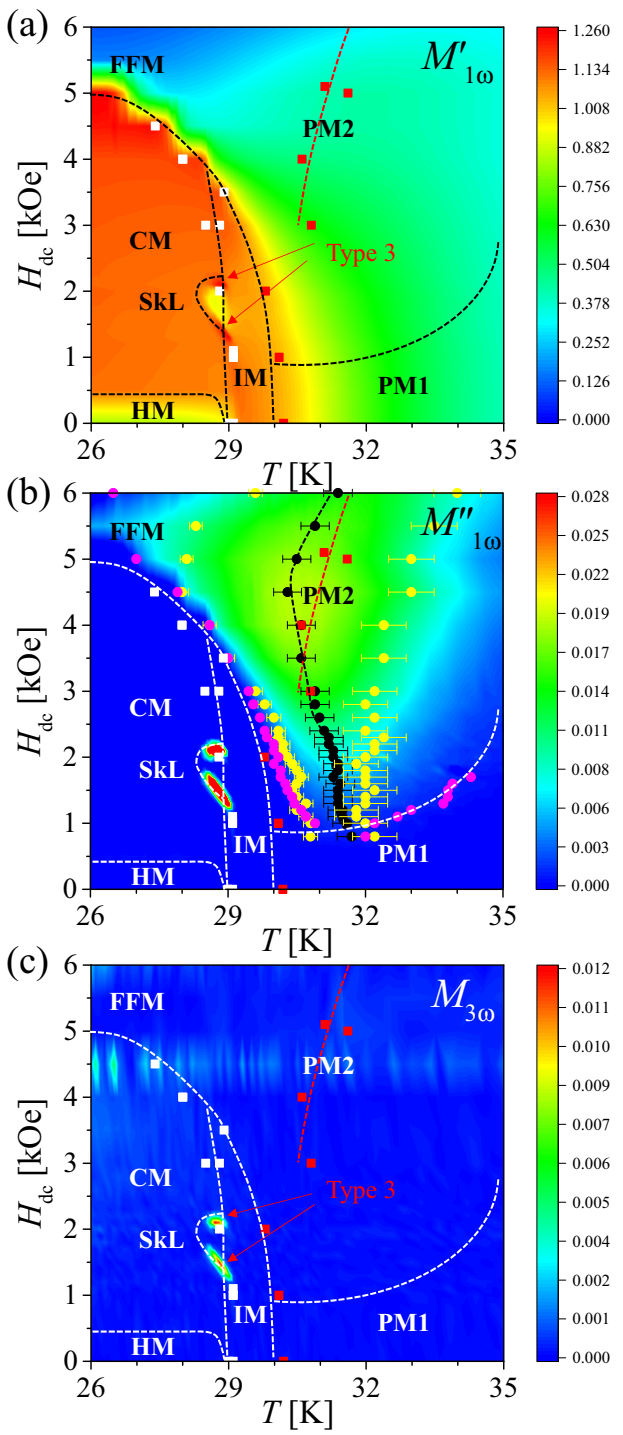

FIG. 7. Intensity maps of $M'_{1\omega}$ (a), $M''_{1\omega}$ (b), and $M_{3\omega}$ (c) for MnSi under an ac field with $h = 3.9$ Oe and $f = 10$ Hz obtained from T-scanning measurements at a fixed H_{dc}. The anomalies observed by the ultrasonic attenuation in the paper of Komatsubara *et al.* [24] were plotted using white and red closed squares in all three figures: White and red data are for the low and high temperature sides of the IM phase, respectively. In (b), black closed circles present the peak position of $M''_{1\omega}$ and yellow ones present those of the maximal and minimal of $dM''_{1\omega}/dT$. Purple closed circles present the data position with the experimentally trustworthy level of $M''_{1\omega} = 8 \times 10^{-4}$ emu/mol that corresponds to approximately 0.1% of the maximum $M'_{1\omega}$.

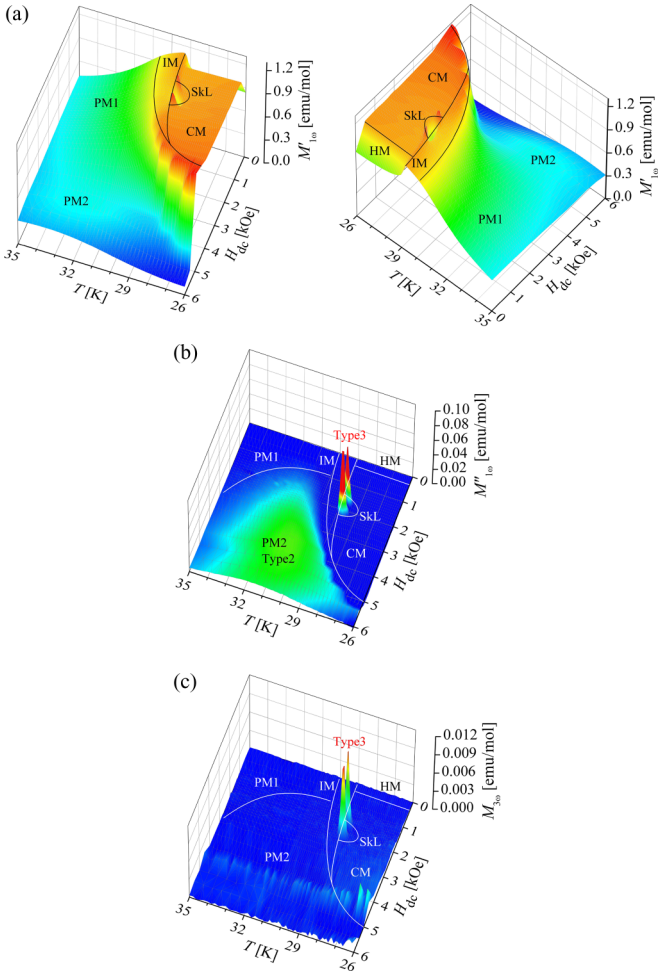

FIG. 8. Three-dimensional Intensity maps of $M'_{1\omega}$ (a), $M''_{1\omega}$ (b), and $M_{3\omega}$ (c) for MnSi under an ac field with $h = 3.9$ Oe and $f = 10$ Hz obtained from T-scanning measurements at a fixed H_{dc}. The physical information is consistent with that of Fig. 7.

anomalies of the ultrasonic attenuation [28]. The existence of a unique region has been noticed as the buildup of strong chiral fluctuating correlation in the neutron experiment by Pappas *et al.* [29]. The above region corresponds to the skyrmion gas (melting state of SkL) region predicted in the film [30]: There might be randomly distributed cylindrical spin vortices with effective mass against the ac magnetic field. It is noted that SkL appears in a narrow H_{dc} region surrounded with the border accompanying prominent $M''_{1\omega}$ and $M_{3\omega}$, where one of multiple DM vectors becomes predominant, resulting in a single domain structure. When we view the appearance of a series of phases in the process of increasing H_{dc}, SkL appears after the appearance of PM2. It may be related that SkL requires thermal fluctuations at the finite H_{dc} [13]: Thermal fluctuation and H_{dc} should suppress the stability of the magnetic equilibrium in cubic chiral magnets. The thermal fluctuation must be sufficient to stabilize the first-order phase transition, and the necessary H_{dc} must be more than the threshold to stabilize PM2 according to the experimental fact. $M_{3\omega}$ observed around the SkL is smaller than that observed in the monoaxial chiral magnet $Cr_{1/3}NbS_2$, suggesting that the pinning of the skyrmions with respect to the crystal lattice is weaker than that of the noncollinear spin

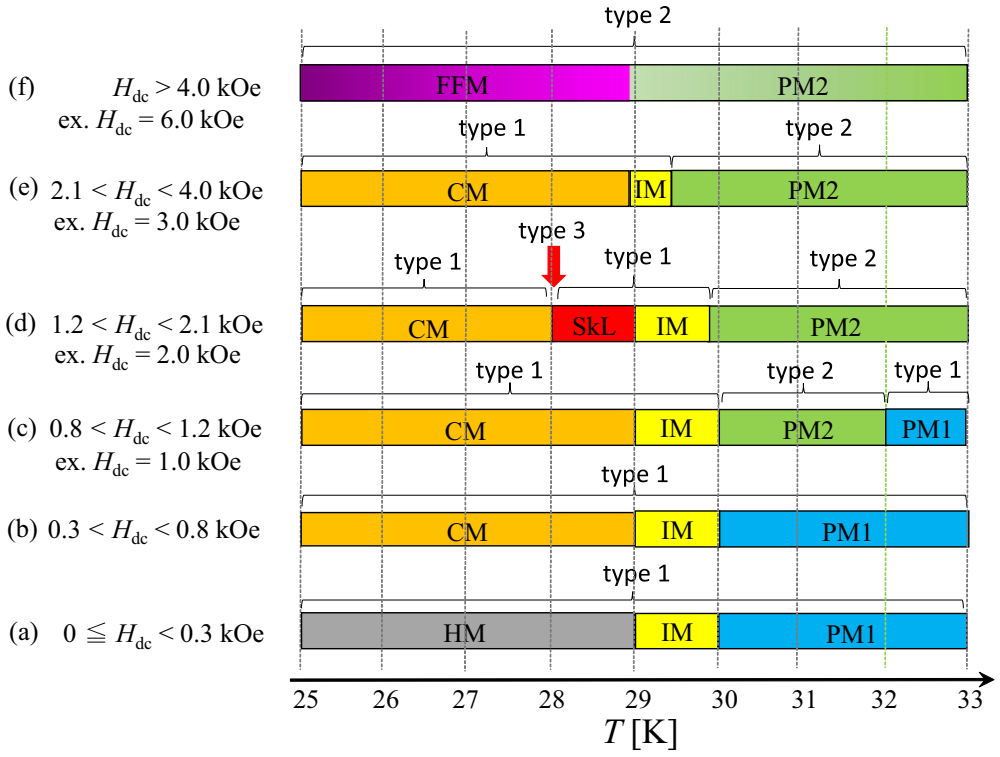

FIG. 9. Change in dynamical magnetic responses as a function of temperature (T) at various dc magnetic fields (H_{dc}'s). The descriptions to characterize the phase or region have been described in the figure caption of Figs. 2 and 7.

textures in $Cr_{1/3}NbS_2$. It has been known that the SkL is further stabilized via the microprocessing for the preparation of thin film [60,61]. However, with the insertion of a defect or disorder in the bulk crystal, the intrinsic creation of noncollinear spin texture should be weakened.

Herein, based on the experimental facts of Figs. 2(b) and 9, we assume an SkL stabilization scenario. First, as H_{dc} increases, the HM phase transforms into CM, and finally to FFM. In PM, there are both PM1 and PM2. H_{dc} stabilizes PM2 accompanying magnetic hysteresis against H_{ac} instead of PM1. Next, the IM phase is stabilized at the boundary between the ordered (HM and CM) and PM (PM1 and PM2) phases via the thermal fluctuation effect. IM has been known to exhibit all the characteristics of a Brazovskii transition [21]. Finally, SkL appears in the low temperature side of IM, and it is stabilized above the extrapolated H_{dc} line of the boundary between PM1 and PM2. Thus, SkL requires a magnetic field fluctuation as well as a thermal fluctuation. Moreover, the former requires the H_{dc} level to be enough to stabilize PM2 near the magnetic ordering temperature.

We discuss which types of system exhibit large nonlinearity in the ac magnetic response [33,49–53], by using Fig. 10. In a symmetric helix such as single-element lanthanoid magnets like Dy [Fig. 10(a)], the competition of exchange interactions brings about the spin helicity. There are many helical domains with right-handed or left-handed helices separated by a domain wall. The $M_{3\omega}$ response is quite small because of its local uniformity of spin-phase order, and its anomaly appears at temperatures where helical pitch changes [51]. The magnitude of $M_{3\omega}$ response of SkL [Fig. 10(c)] is in the same level of glassy systems [44,49,50], and that of multiple DM HM [Fig. 10(b)] detected by the H_{dc} scanning is smaller than that of SkL: The domain network of SkL with small pinning to the lattice is uniform. This 2D vortex lattice is the quasistable state stabilized by both thermal fluctuation and external H_{dc}, and there is no uniaxial magnetic anisotropy. The monoaxial chiral magnet (i.e. single DM HM) [Fig. 10(e)] exhibits the spatially uniform helical domains along the helical

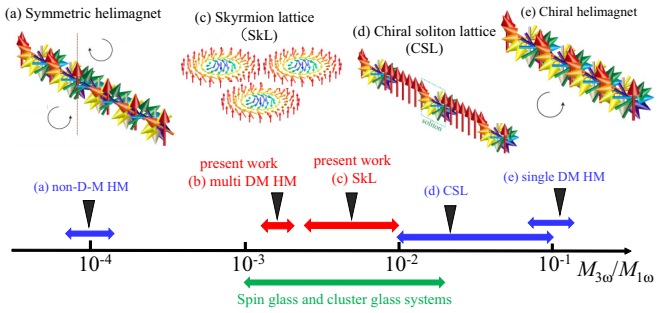

FIG. 10. Overview of robustness of noncollinear spin textures, evaluated via the Klirr factor $M_{3\omega}/M_{1\omega}$. (a) Symmetric helix in which two chiralities, such as left-handed and right-handed helicities, coexist across a domain boundary [51]. Four examples based on the DM vector are presented: (b) Multiple DM helimagnet (HM) (present work). (c) Skyrmion lattice (SkL) (2D lattice of spin vortices, present work). (d) Chiral soliton lattice (CSL), a magnetic superlattice formed in a monoaxial chiral magnet at H_{dc} [33]. (e) Chiral magnet in which there is only a single type of helicity such as left-handed or right-handed (single DM HM) [33,52,53]. For reference, $M_{3\omega}/M_{1\omega}$ for spin glass and cluster glass systems are also shown [44,49,50].

direction. The uniformity of the monoaxial helicity is known to be physically robust via the Lorentz TEM observations on $Cr_{1/3}NbS_2$ [6]. Indeed, the nonlinear response of monoaxial chiral magnets is huge. In the CSL constructed by inserting the helical domain walls to HM state [Fig. 10(d)], the FM region increases by increasing H_{dc}, so that the $M_{3\omega}$ response increases with decreasing the number of domain walls. The magnitude of $M_{3\omega}$ response of CSL is located between SkL and single DM HM. Thus, defects, disorders, randomness, domain walls, and so on reduce the uniformity of the chiral phase coherence. Of course, this idea is adopted to the SkL phase of MnSi. The aforementioned general defects generate smaller SkL islands, between which any glassy behavior may appear due to the competition of any effective anisotropy vectors of vortex lattices. However, its glassy feature would be small. Looking from the opposite side, with increasing uniformity and nonlocality of the chiral phase coherence, the nonlinearity of the magnetic response increases, resulting in robust noncollinear spin texture.

VI. CONCLUSION

We verified the phase diagram of the cubic chiral magnet MnSi as a function of T and H_{dc} using two- and three-dimensional intensity mappings of the ac magnetic responses. In terms of the magnetic dynamics, the vortices lattice of SkL exhibits a nonlinear magnetic response at the boundary with the CM phase, where the magnitude is much smaller than CSL consisting of kink type of topological objects in the monoaxial chiral magnet $Cr_{1/3}NbS_2$, suggesting that the spatial rigidity of the spin vortex in the SkL phase is weaker than that of the monoaxial spin texture in the single DM system. The HM phase in multiple DM system exhibits a smaller third-harmonic response than the HM one in the single DM system. In the T-increasing process, the creation of skyrmions at the border between CM and SkL phases prominently exhibits nonlinear magnetic behavior. Furthermore, it is steady even against the ac magnetic field with high frequency. By contrast, the annihilation of skyrmions at the border between SkL and IM phases shows perfect linear behavior, suggesting that the pinning of skyrmion lattice with respect to the crystal lattice against heating is weak. In addition to the evaluation of the noncollinear textures of the SkL phases, by using the two- and three-dimensional intensity mappings of $M''_{1\omega}$, we verified a new PM region termed PM2, whose magnetic dynamics is similar to that of the FFM region. Thus, the PM2 region originating from any magnetic domain formation is distinguished from PM1 with a linear ac response, and it appears in the wide T-H_{dc} region where the second harmonic resistivity due to spin fluctuation is observed and the skyrmion gas phase in the film is predicted.

ACKNOWLEDGMENTS

The authors thank Y. Kato for valuable discussion. This work was supported by Grants-in-Aid for Scientific Research, Grants No. (A) 18205023 and No. (S) 25220803, from the Ministry of Education, Culture, Sports, Science and Technology (MEXT), Japan. This work was also supported by CResCent (Chirality Research Center) in Hiroshima University (the MEXT program for promoting the enhancement of research universities, Japan) and the JSPS Core-to-Core Program, A. Advanced Research Networks.

[1] N. Manton and P. Sutcliffe, *Topological Solitons* (Cambridge University Press, Cambridge, 2007).
[2] I. E. Dzyaloshinskii, J. Phys. Chem. Solid **4**, 241 (1958).
[3] T. Moriya, Phys. Rev. **120**, 91 (1960).
[4] J. Kishine, K. Inoue, and Y. Yoshida, Prog. Theor. Phys. Suppl. **159**, 82 (2005).
[5] B. J. Chapman, A. C. Bornstein, N. J. Ghimire, D. Mandrus, and M. Lee, Appl. Phys. Lett. **105**, 072405 (2014).
[6] Y. Togawa, T. Koyama, K. Takayanagi, S. Mori, Y. Kousaka, J. Akimitsu, S. Nishihara, K. Inoue, A. S. Ovchinnikov, and J. Kishine, Phys. Rev. Lett. **108**, 107202 (2012).
[7] A. O. Leonov, T. L. Monchesky, N. Romming, A. Kubetzka, A. N. Bogdanov, and R. Wiesendanger, New J. Phys. **18**, 065003 (2016).
[8] D. McGrouther, R. J. Lamb, M. Krajnak, S. McFadzean, S. McVitie, R. L. Stamps, A. O. Leonov, A. N. Bogdanov, and Y. Togawa, New J. Phys. **18**, 095004 (2016).
[9] A. N. Bogdanov and D. A. Yablonskii, Sov. Phys. JETP **68**, 101 (1989).
[10] A. Bogdanov and A. Hubert, J. Magn. Magn. Mater. **138**, 255 (1994).
[11] A. Bogdanov and A. Hubert, J. Magn. Magn. Mater. **195**, 182 (1999).
[12] U. K. Rößler, A. A. Leonov, and A. N. Bogdanov, J. Phys. Conf. Ser. **303**, 012105 (2011).
[13] S. Muhlbauer, B. Binz, F. Jonietz, C. Pfleiderer, A. Rosch, A. Neubauer, R. Georgii, and P. Boni, Science **323**, 915 (2009).
[14] T. Adams, S. Mühlbauer, C. Pfleiderer, F. Jonietz, A. Bauer, A. Neubauer, R. Georgii, P. Böni, U. Keiderling, K. Everschor *et al.*, Phys. Rev. Lett. **107**, 217206 (2011).
[15] X. Z. Yu, Y. Onose, N. Kanazawa, J. H. Park, J. H. Han, Y. Matsui, N. Nagaosa, and Y. Tokura, Nature (London) **465**, 901 (2010).
[16] X. Z. Yu, N. Kanazawa, Y. Onose, K. Kimoto, W. Z. Zhang, S. Ishiwata, Y. Matsui, and Y. Tokura, Nat. Mater. **10**, 106 (2011).
[17] S. Seki, X. Z. Yu, S. Ishiwata, and Y. Tokura, Science **336**, 198 (2012).
[18] N. Romming, C. Hanneken, M. Menzel, J. E. Bickel, B. Wolter, K. von Bergmann, A. Kubetzka, and R. Wiesendanger, Science **341**, 636 (2013).
[19] N. Romming, A. Kubetzka, C. Hanneken, K. von Bergmann, and R. Wiesendanger, Phys. Rev. Lett. **114**, 177203 (2015).
[20] Y. Ishikawa, G. Shirane, J. A. Tarvin, and M. Kohgi, Phys. Rev. B **16**, 4956 (1977).
[21] A. Bauer and C. Pfleiderer, Phys. Rev. B **85**, 214418 (2012).
[22] H. Wilhelm, M. Baenitz, M. Schmidt, U. K. Rößler, A. A. Leonov, and A. N. Bogdanov, Phys. Rev. Lett. **107**, 127203 (2011).

[23] T. Schwarze, J. Waizner, M. Garst, A. Bauer, I. Stasinopoulos, H. Berger, C. Pfleiderer, and D. Grundler, Nat. Mater. **14**, 478 (2015).

[24] S. Kusaka, K. Yamamoto, T. Komastubara, and Y. Ishikawa, Solid State Commun. **20**, 925 (1976).

[25] A. E. Petrova and S. M. Stishov, Phys. Rev. B **91**, 214402 (2015).

[26] H. Wilhelm, M. Baenitz, M. Schmidt, C. Naylor, R. Lortz, U. K. Rößler, A. A. Leonov, and A. N. Bogdanov, J. Phys.: Condens. Matter **24**, 294204 (2012).

[27] A. Bauer, M. Garst, and C. Pfleiderer, Phys. Rev. Lett. **110**, 177207 (2013).

[28] T. Yokouchi, N. Kanazawa, A. Kikkawa, D. Morikawa, K. Shibata, T. Arima, Y. Taguchi, F. Kagawa, and Y. Tokura, Nat. Commun. **8**, 866 (2017).

[29] C. Pappas, L. J. Bannenberg, E. Lelièvre-Berna, F. Qian, C. D. Dewhurst, R. M. Dalgliesh, D. L. Schlagel, T. A. Lograsso, and P. Falus, Phys. Rev. Lett. **119**, 047203 (2017).

[30] M. Ezawa, Phys. Rev. B **83**, 100408(R) (2011).

[31] C. Pappas, E. Lelièvre-Berna, P. Falus, P. M. Bentley, E. Moskvin, S. Grigoriev, P. Fouquet, and B. Farago, Phys. Rev. Lett. **102**, 197202 (2009).

[32] C. Pappas, E. Lelièvre-Berna, P. Bentley, P. Falus, P. Fouquet, and B. Farago, Phys. Rev. B **83**, 224405 (2011).

[33] K. Tsuruta, M. Mito, H. Deguchi, J. Kishine, Y. Kousaka, J. Akimitsu, and K. Inoue, Phys. Rev. B **93**, 104402 (2016).

[34] Y. Kimura, T. Sako, and R. Hayakawa, Ferroelectrics **147**, 315 (1993).

[35] H. Orihara, A. Fukase, S. Izumi, and Y. Ishibashi, Ferroelectrics **147**, 411 (1993).

[36] Y. Kimura and R. Hayakawa, Jpn. J. Appl. Phys. **32**, 4571 (1993).

[37] K. Obayashi, H. Orihara, and Y. Ishibashi, J. Phys. Soc. Jpn. **64**, 3188 (1995).

[38] Y. Kimura, R. Hayakawa, N. Okabe, and Y. Suzuki, Phys. Rev. E **53**, 6080 (1996).

[39] Y. Kimura, H. Isono, and R. Hayakawa, Phys. Rev. E **64**, 060701(R) (2001).

[40] Y. Kimura, H. Isono, and R. Hayakawa, Eur. Phys. J. E **9**, 3 (2002).

[41] M. Mito, H. Matsui, K. TsurutaF, H. Deguchi, J. Kishine, K. Inoue, Y. Kousaka, S. Yano, Y. Nakao, and J. Akimitsu, J. Phys. Soc. Jpn. **84**, 104707 (2015).

[42] M. Suzuki, Prog. Theor. Phys. **58**, 1151 (1977).

[43] S. Fujiki and S. Katsura, Prog. Theor. Phys. **65**, 1130 (1981).

[44] Y. Miyako, S. Shikazawa, T. Saito, and Y. G. Yuochunas, J. Phys. Soc. Jpn. **46**, 1951 (1979).

[45] T. Bitoh, T. Shirane, and S. Chikazawa, J. Phys. Soc. Jpn. **62**, 2837 (1993).

[46] T. Shirane, T. Moiya, T. Bitoh, A. Sawada, H. Aida, and S. Chikazawa, J. Phys. Soc. Jpn. **64**, 951 (1995).

[47] T. Shirane and S. Sakurai, J. Korean Phys. Soc. **62**, 2173 (2013).

[48] S. Chikazumi, *Physics of Ferromagnets* (Oxford University Press, New York, 1997).

[49] M. Mito, M. Ogawa, H. Deguchi, M. Yamashita, and H. Miyasaka, J. Appl. Phys. **107**, 124316 (2010).

[50] M. Mito, M. Ogawa, H. Deguchi, M. Yamashita, and H. Miyasaka, J. Phys. Soc. Jpn. **81**, 064716 (2012).

[51] M. Mito, K. Iriguchi, Y. Taniguchi, M. Kawase, S. Takagi, and H. Deguchi, J. Phys. Soc. Jpn. **80**, 064707 (2011).

[52] M. Mito, K. Iriguchi, H. Deguchi, J.-i. Kishine, K. Kikuchi, H. Ohsumi, Y. Yoshida, and K. Inoue, Phys. Rev. B **79**, 012406 (2009).

[53] M. Mito, K. Iriguchi, H. Deguchi, J. Kishine, Y. Yoshida, and K. Inoue, J. Appl. Phys. **111**, 103914 (2012).

[54] T. Liu, H. Zheng, S. Kang, Y. Shiota, S. Hayami, M. Mito, O. Sato, K. Yoshizawa, S. Kanegawa, and C. Duan, Nat. Commun. **4**, 2826 (2013).

[55] Y. Kousaka, N. Ikeda, T. Ogura, T. Yoshii, J. Akimitsu, K. Ohishi, J.-i. Suzuki, H. Hiraka, M. Miyagawa, S. Nishihara *et al.*, JPS Conf. Proc. **2**, 010205 (2014).

[56] M. N. Wilson, A. B. Butenko, A. N. Bogdanov, and T. L. Monchesky, Phys. Rev. B **89**, 094411 (2014).

[57] S. V. Grigoriev, S. V. Maleyev, A. I. Okorokov, Y. O. Chetverikov, and H. Eckerlebe, Phys. Rev. B **73**, 224440 (2006).

[58] Y. Nii, T. Nakajima, A. Kikkawa, Y. Yamasaki, K. Ohishi, J. Suzuki, Y. Taguchi, T. Arima, Y. Tokura, and Y. Iwasa, Nat. Commun. **6**, 8539 (2015).

[59] A. Chacon, A. Bauer, T. Adams, F. Rucker, G. Brandl, R. Georgii, M. Garst, and C. Pfleiderer, Phys. Rev. Lett. **115**, 267202 (2015).

[60] M. N. Wilson, E. A. Karhu, A. S. Quigley, U. K. Rößler, A. B. Butenko, A. N. Bogdanov, M. D. Robertson, and T. L. Monchesky, Phys. Rev. B **86**, 144420 (2012).

[61] X. Yu, A. Kikkawa, D. Morikawa, K. Shibata, Y. Tokunaga, Y. Taguchi, and Y. Tokura, Phys. Rev. B **91**, 054411 (2015).